Spectroscopic Characterization of the NO Adduct of Hydroxylamine Oxidoreductase†

Michael P. Hendrich,*,‡ Anup K. Upadhyay,‡ Jeanne Riga,‡ David M. Arciero,§ and Alan B. Hooper§

Department of Chemistry, Carnegie Mellon University, Pittsburgh, Pennsylvania 15213, and Department of Biochemistry, Molecular Biology and Biophysics, University of Minnesota, St. Paul, Minnesota 55108

Received June 26, 2001; Revised Manuscript Received February 11, 2002

ABSTRACT: Hydroxylamine oxidoreductase (HAO) from the autotrophic nitrifying bacterium *Nitrosomonas europaea* catalyzes the oxidation of NH_2OH to NO_2^-. The enzyme contains eight hemes per subunit which participate in catalysis and electron transport. NO is found to bind to the enzyme and inhibit electron flow to the acceptor protein, cytochrome c_{554}. NO is found to oxidize either partially or fully reduced HAO, but NO will not reduce ferric HAO. Since NO can be reduced but not oxidized to product by HAO, NO is not considered to be a long-lived intermediate in the catalytic mechanism. Substrate oxidation occurs in the presence of bound NO or cyanide, suggesting a second interaction site for substrate with HAO and providing a means for recovery of the NO-inhibited form of the enzyme. Upon addition of NO to oxidized HAO, the integer-spin EPR signal from the active site vanishes, an IR band from NO appears at 1920 cm^{-1}, and a diamagnetic quadrupole iron doublet appears in Mössbauer spectroscopy with $\delta = 0.06$ mm/s and $\Delta Eq = 2.1$ mm/s. The NO stretching frequency and Mössbauer parameters are characteristic of an $\{FeNO\}^6$ heme complex. New Mössbauer data on ferric myoglobin−NO are also presented for comparison. The results indicate that NO binds to heme P460 and that the loss of the integer-spin EPR signal is due to the conversion of heme P460 to a diamagnetic $S = 0$ state and concomitant loss of magnetic interaction with neighboring heme 6. In previous studies where the heme P460−heme 6 interaction was affected by substrate or cyanide binding, a signal attributable to heme 6 was not observable. In contrast, in this work, the NO-induced loss of the signal is accompanied by the appearance of a previously unobserved large g_{max} (or HALS) low-spin EPR signal from heme 6.

The autotrophic bacterium, *Nitrosomonas europaea*, derives energy for growth from the oxidation of ammonia to nitrite. The pathway for this process contains two enzymes, ammonia monooxygenase (AMO)[1] and hydroxylamine oxidoreductase (HAO) (*1*). AMO, a membrane-bound enzyme, catalyzes the oxidation of ammonia in the reaction $NH_3 + O_2 + 2e^- + 2H^+ \rightarrow NH_2OH + H_2O$. HAO, a soluble enzyme found in the periplasm, catalyzes the reaction $NH_2OH + H_2O \rightarrow NO_2^- + 4e^- + 5H^+$, as well as the oxidation of hydrazine to dinitrogen (*2*, *3*). The reducing equivalents generated in the oxidation of hydroxylamine are the starting point for essential electron transfer to the tetraheme cytochrome c_{554}, ubiquinone, a bc_1 complex, and cytochrome oxidase processes leading to ATP synthesis, reverse electron flow to $NADP^+$, and return of electrons to the primary monooxygenase reaction (*1*). An HAO with very similar molecular and catalytic properties is found in the organism responsible for anaerobic ammonium oxidation where the growth-supporting reaction is $NH_4^+ + NO_2^- \rightarrow N_2 + 2H_2O$ with hydrazine as intermediate (*4*). HAO is thought to catalyze the production of N_2 from N_2H_4 and possibly also reduce nitrite to an *N*-oxide precursor of one of the two nitrogens of hydrazine.

The crystal structure of HAO shows a trimer of polypeptides with each monomer (68 kDa) (*5*, *6*) containing eight hemes covalently bound via two cysteine thioether linkages in the CXYCH sequences, for a total of 24 hemes per protein (*7*). Seven of these are *c*-type hemes, while the eighth is an unusual prosthetic group, termed heme P460, which displays a Soret band at 463 nm for the reduced form of HAO. The arrangement in space and numbering of the hemes of a single polypeptide chain are shown in Figure 1. HAO belongs to a growing family of structurally well-characterized bacterial multiheme proteins involved in electron transfer and redox chemistry of small inorganic molecules. These proteins contain conserved structural arrangements of heme centers, despite significant differences in primary sequence and protein architecture. The heme organization within a subunit of HAO is comprised of a triheme cluster (hemes P460, 6, and 7), four other hemes are involved in two diheme clusters (hemes 1 and 2, and hemes 3 and 5), and one heme is not part of a cluster (heme 8). The conserved structural arrangements were first identified when the structure of cytochrome c_{554} from *Nitrosomonas* was reported (*8*) and further observed

† Supported by grants from the National Institutes of Health, GM-49970 (M.P.H.), and the National Science Foundation, MCB-9723608 (A.B.H.).

* Corresponding author. Phone: (412) 268-1058. Fax: (412) 268-1061. E-mail: hendrich@andrew.cmu.edu.

‡ Carnegie Mellon University.

§ University of Minnesota.

[1] Abbreviations: AMO, ammonia monooxygenase; HAO, hydroxylamine oxidoreductase; TPP, tetraphenylporphyrin; HALS, highly anisotropic low spin; DEANO, 2-(*N*,*N*-diethylamino)diazenolate 2-oxide; $\{FeNO\}^n$, see ref *33*.

10.1021/bi011332z CCC: $22.00
Published on Web 03/12/2002

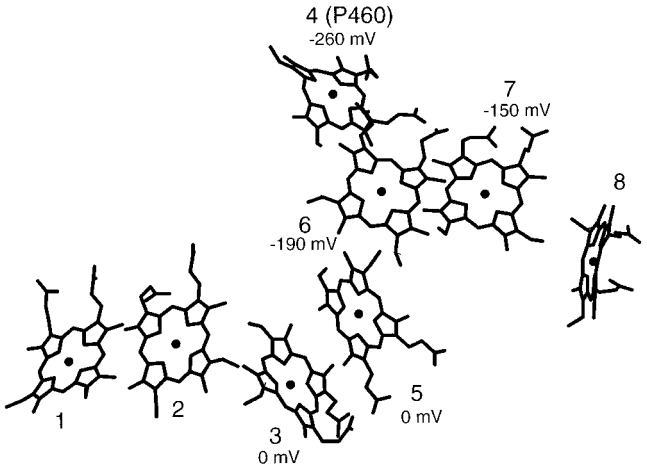

FIGURE 1: Spatial arrangement of hemes from the crystal structure in a monomeric unit of HAO. The heme numbering scheme and assignments of various heme midpoint potentials are shown.

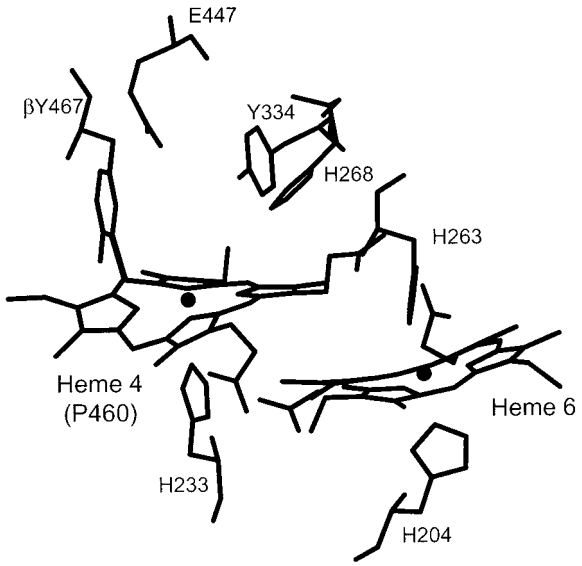

FIGURE 2: Substrate binding site of HAO.

in the structure of the pentaheme nitrite reductase from *Sulfurospirillum deleyianum* (*9*). On the basis of recent EPR spectroscopic correlations to the structure of HAO, we have made assignment of midpoint reduction potentials to five of the eight hemes shown in Figure 1 (*10*, *11*). The three unassigned hemes have midpoint potentials of +288, −265, and −412 mV vs NHE.[2]

The function of the *c*-hemes is believed to be the transfer of electrons from the catalytic site to the binding site of the electron acceptor cytochrome c_{554} (*12*, *13*). Several observations indicate that heme P460 is a component of the active site of HAO, shown in Figure 2. Treatment of oxidized HAO with H_2O_2 causes loss of hydroxylamine reactivity and concomitant irreversible loss of the absorbency of ferrous P460, whereas the optical spectra of the *c*-hemes are unaffected (*14*). An integer-spin EPR signal, which originates from heme P460, vanishes in the presence of either substrates or cyanide (*15*). Formation of the cyanide−HAO complex results in noncompetitive inhibition of hydroxylamine oxidation, inhibition of the reaction of ferric HAO with H_2O_2, and inhibition of the inactivation of HAO by organohydrazine suicide substrates (*16*).

Heme P460 of HAO appears to be derived from a *c*-heme with typical covalent thioether linkages to Cys229 and Cys232 but also possesses a unique third covalent linkage between the 5-*meso* carbon of the porphyrin and the C3 ring carbon of Tyr467 (*6*, *17*). The tyrosine is from the polypeptide chain of an adjacent subunit and thus cross-links the subunits. Heme P460 is exchange coupled to heme 6 (*11*). Heme 6, like all the hemes in HAO except P460, has axial bis-His coordination. Heme P460 has one axial His ligand and an open axial site for coordination of substrate. The substrate binding pocket consists of Tyr467 and three other protein residues, as shown in Figure 2. The three other residues, Glu447, Tyr334, and His268, are on the same peptide chain as heme P460 and heme 6. The distances to the nearest carboxylate O, phenolate O(334), phenolate O(467), and imidazole N are 8.0, 6.0, 3.7, and 4.9 Å, respectively. The novel structure of heme P460 may be responsible for its unusual electronic properties. Mössbauer spectroscopy of fully reduced HAO shows ferrous P460 to be high spin and to exhibit an unusually large quadrupole splitting ($\Delta Eq = 4.21$ mm/s); thus the iron atom experiences the largest electric field gradient of any known naturally occurring ferrous heme (*18*). Resonance Raman spectroscopy of ferrous P460 confirms that the band at 463 nm is a Soret band and that it is a unique heme with symmetry lower than those of protoporphyrin IX or chlorins (*19*).

Stepwise oxidation of hydroxylamine may proceed through the sequence: $NH_2OH \rightarrow HNO \rightarrow NO \rightarrow NO^+ \rightarrow HNO_2$, where the first three steps represent 2, 1, and 1 electron oxidations, respectively, and the final step represents condensation of nitrosonium with H_2O. In a competing model, the oxidation may occur by successive two-electron steps where NO would not be an intermediate. Some evidence supports the possibility that NO is an intermediate and thus supports the first model. Whereas in aerobic cells of *Nitrosomonas* hydroxylamine is converted stoichiometrically to nitrite, purified HAO will catalyze the oxidation of hydroxylamine to HNO (as seen by the production of N_2O) and to NO (*20*, *21*). In these studies, NO was shown not to be produced by the reduction of nitrite. Production of N_2O and NO from hydroxylamine has also been observed with the HAO of Annamox (*4*). It has not been possible to demonstrate the conversion of NO to nitrite by HAO; hence the evidence for NO as an intermediate is inconclusive.

All eight hemes of fully reduced HAO can be reoxidized during the reduction of O_2 (*22*) or H_2O_2 (*23*) at the heme P460 active site. Preparations of purified HAO were shown to catalyze the stoichiometric reduction of nitrite and oxidation of hydroxylamine to yield N_2O, $NH_2OH + HNO_2 \rightarrow N_2O + 2H_2O$, suggesting that HAO could withdraw two electrons from hydroxylamine, release nitroxyl, bind nitrite, and reduce the latter to nitroxyl (*24*). Correspondingly, in aerobic reaction mixtures the steady-state level of reduction of *c*-hemes of dithionite-reduced HAO was diminished by the addition of nitrite (*25*, *26*). Likewise, the hydroxylamine- or hydrazine-reduced *c*-hemes of the Annamox HAO are reported to be reoxidized by added NO or nitrite, and with reduced methyl viologen as electron donor, Annamox HAO is reported to reduce nitrite to N_2O and NO (*4*). Taken together, work to date indicates that removal of the final one

[2] All potentials quoted in this paper are reduction potentials versus NHE.

electron and/or two electrons in the production of nitrite by HAO may be reversible.

Given the apparent ability of HAO to catalyze the oxidative and reductive production of NO and possibly the reduction of NO and the theoretical capability of HAO to catalyze the oxidation of NO, the interaction with HAO has been studied in the present work. As a small ligand, nitric oxide has long been a useful probe of iron and heme complexes (*27*), and relevant analytical methods are IR (*28*, *28*), EPR (*30*, *31*), and Mössbauer (*32*) spectroscopies. NO is a radical which upon coordination converts an overall even-electron system to an odd-electron system. Furthermore, NO adducts of heme complexes have characteristic IR absorption bands allowing determination of the electronic state with comparison to well-characterized proteins. The data presented here indicate adduct formation to heme P460 and that NO is not a long-lived intermediate in the enzymatic cycle. We observe formation of $\{FeNO\}^6$ and $\{FeNO\}^7$ complexes of HAO (*33*).[3] The formation of the NO adduct of heme P460 allowed, for the first time, the observation of a large g_{max} EPR signal from heme 6, the heme exchange coupled to heme P460 in the resting enzyme. The hemes that show this large g_{max} EPR signal are also referred to as highly anisotropic low-spin hemes (HALS).

MATERIALS AND METHODS

Purification of Enzyme. Growth and ^{57}Fe enrichment of *N. europaea* and purification of HAO were as described previously (*13*, *16*, *18*). All experiments were performed in 50 mM potassium phosphate buffer, pH 7.5, unless otherwise noted. The concentration of HAO was determined spectrophotometrically for the oxidized state ($\epsilon = 700$ mM^{-1} cm^{-1} at 408 nm) and is given in terms of the subunit concentration (68 kDa) throughout this paper. All chemicals were of reagent grade or better. Double distilled or Millipore Super Q water was used throughout. NO samples unless otherwise stated were prepared by bubbling NO gas (Matheson) first through a degassed concentrated solution of NaOH and then into samples of HAO degassed with Ar. Samples prepared with $Na_2S_2O_4$ were degassed with Ar. For one EPR sample, the NO donor agent, DEANO Na salt (Alexis Biochemicals, $t_{1/2} = 16$ min, CAS 86831-65-4), was added to a sample of HAO degassed with Ar.

FTIR Spectroscopy. The infrared measurements were performed on a Mattson Infinity Series 60AR FTIR spectrometer purged with N_2 gas and using an InGaAs detector. Each spectrum was the average of 32 scans at a resolution setting of 2 cm^{-1} with mirror speeds of 10 kHz forward and 12.5 kHz reverse. A SL-2 CaF_2 sealed IR cell of path length 0.025 mm (International Crystal Laboratories) was used in all experiments. Samples of degassed HAO were prepared by buffer exchange with 10 mM KP_i in 97% D_2O. The NO samples were prepared by bubbling ^{14}NO gas (Matheson) first through a degassed concentrated solution of NaOH/D_2O and then into degassed samples of HAO. To prepare the ^{15}NO gas, $K^{15}NO_2$ (Isotec) and KI (Fischer) were mixed in a 4:1 ratio in a 5 mL glass vial, and 0.5 mL of water was added dropwise. Sulfuric acid (50%, Fischer) was then added dropwise to the mixture to produce ^{15}NO gas. The evolved gas was passed through a concentrated degassed solution of NaOH/D_2O and then into a degassed sample of HAO.

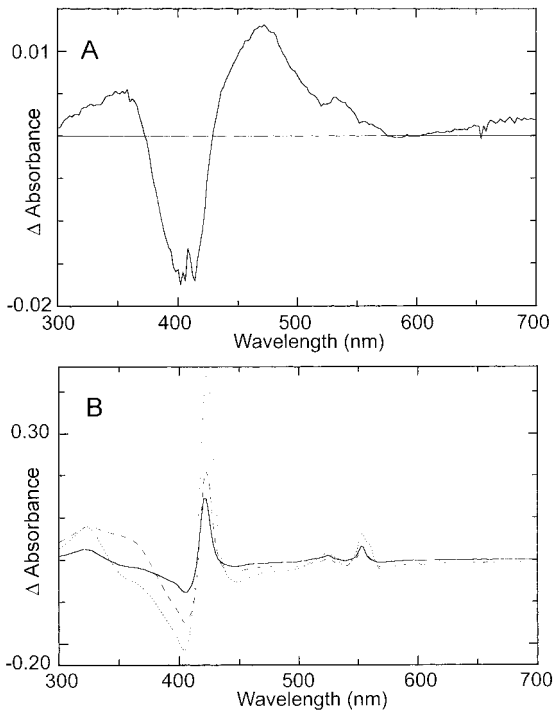

FIGURE 3: Optical changes associated with binding of NO to HAO (A) and effect of NO on reduction of *c*-hemes of HAO by hydrazine (B). (A) Difference spectrum, (HAO + NO) minus (HAO), occurring after NO gas was bubbled through a solution of HAO. (B) Difference spectra of {(HAO + NO) + N_2H_4} minus {HAO + NO} (solid line), {HAO + N_2H_4} minus {HAO} (dotted line), and {(HAO + N_2H_4) + NO} minus {HAO} (dashed line). [HAO] = 1.5 μM; [N_2H_4] = 2 mM; the spectrum of {(HAO + N_2H_4) + NO} minus {HAO} was recorded after 3 min; the buffer was 50 mM potassium phosphate, pH 7.0.

EPR Spectroscopy. X-band EPR spectra were recorded on a Bruker 300 spectrometer equipped with an Oxford ESR-910 liquid helium cryostat and a Bruker bimodal cavity. The quantification of all signals is relative to a CuEDTA spin standard. Unless otherwise stated, the spectra were obtained with a field modulation of 1 mT_{pp} at 100 kHz. The magnetic field was calibrated with an NMR gaussmeter, and the microwave frequency was measured with a counter.

Mössbauer Spectroscopy. Mössbauer spectra were obtained on a constant acceleration instrument, and isomeric shifts are reported relative to an iron metal standard. The available temperature range is 1.5−250 K, and a magnetic applied field of up to 45 mT can be applied to the sample.

RESULTS

UV−Visible Spectroscopy. Optical changes associated with NO binding to HAO are shown in Figure 3A. The difference spectrum shows a decrease in absorbance near 405 nm and a concomitant increase near 465 nm. The change in molar absorptivity is about 7 mM^{-1} cm^{-1} per P460 heme of HAO, a value in the same range as that observed for the binding of cyanide to HAO (*16*).

FTIR Spectroscopy. The FTIR spectrum of 1.5 mM oxidized HAO (all ferric iron) in 10 mM KP_i and D_2O, pD 6.7, versus D_2O is shown in the inset of Figure 4. The bands at 1650, 1550, and 1450 cm^{-1} are vibrations from the peptide

[3] For the nomenclature $\{FeNO\}^n$, *n* refers to the number of iron d-electrons plus the one unpaired NO electron.

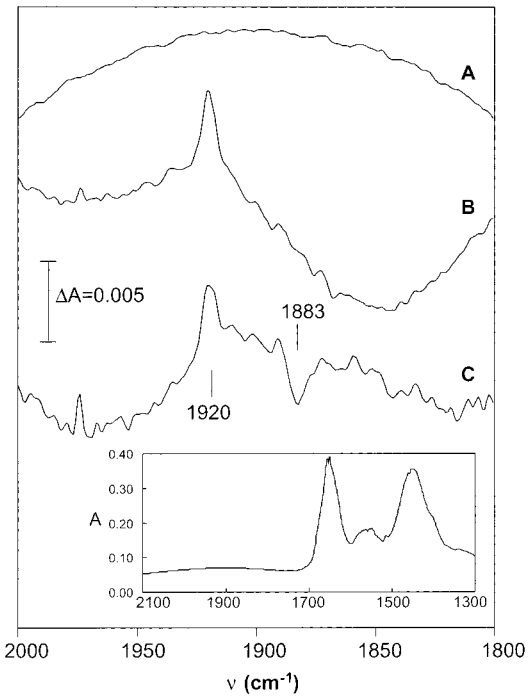

FIGURE 4: FTIR spectra of 1.5 mM oxidized HAO in 10 mM KP_i and D_2O, pD 6.7. The inset shows a broad wavelength scan of HAO. (A) Prior to NO addition. (B) After NO addition. (C) Difference spectra of ^{14}NO minus ^{15}NO.

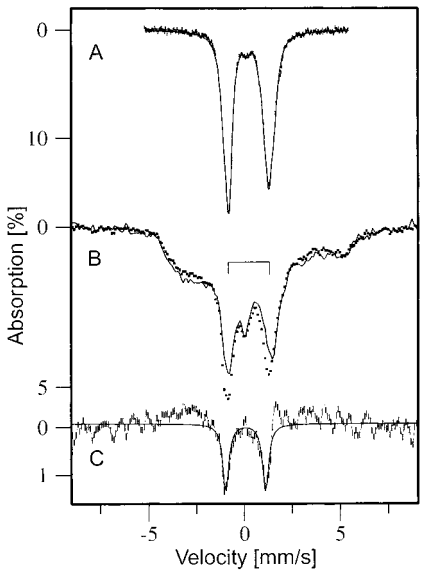

FIGURE 5: (A) Mössbauer spectra of 1 mM oxidized ^{57}Fe HAO recorded at 150 K in zero magnetic field. The least-squares fit (solid line) overlaid on the data is for three species: $\delta = 0.24$ mm/s, $\Delta Eq = 2.29$ mm/s (78%), $\delta = 0.18$ mm/s, $\Delta Eq = 1.89$ mm/s (19%), and $\delta = 0.48$ mm/s, $\Delta Eq = 0.63$ mm/s (3%). (B) Oxidized HAO (solid line) and NO-treated HAO (dots) both recorded at 4.2 K with an applied magnetic field of 45 mT parallel to the gamma beam direction. (C) Difference spectrum of (B) showing HAO + NO minus HAO. The least-squares fit (sold line) for one species gives $\delta = 0.04$ mm/s, $\Delta Eq = 2.00$ mm/s, and $\Gamma = 0.47$ mm/s, accounting for 8% of total iron.

backbone which typically dominate IR spectra of proteins. Figure 4A is an expanded plot of the oxidized HAO spectrum showing the baseline above 1800 cm^{-1}. Figure 4B shows the result of addition of NO to an anaerobic sample of protein. A new band is observed at 1920 cm^{-1} with an absorbance of 0.0042 and a full width at half-maximum (fwhm) of 6 cm^{-1}. This band remains unchanged for at least 3 h from the initial spectral recording. To verify that the new band is from an NO species, an equivalent sample was prepared with ^{15}NO. The difference FTIR spectrum $^{14}NO - {}^{15}NO$ is shown in Figure 4C. The band at 1920 cm^{-1} vanishes, and a new band is observed at 1883 cm^{-1}. The observed shift of 37 cm^{-1} is in approximate agreement with the theoretical calculated shift of 34.5 cm^{-1}. The sample of HAO + NO was purged of NO by flushing with Ar during illumination with white light (300 W projection bulb) while in a room temperature water bath. After this treatment, the band at 1920 cm^{-1} vanished.

Control experiments were performed on a solution sample of sperm whale myoglobin in 100 mM KP_i and D_2O, pD 6.7. In the presence of NO, a band appeared at 1922 cm^{-1} with an absorbance of 0.0054 and fwhm of 10 cm^{-1}. The addition of ^{15}NO resulted in a band 37 cm^{-1} lower at 1885 cm^{-1}. In contrast to HAO, the NO band in myoglobin gradually disappeared and vanished within 30 min from the initial spectral recording. This is due to reductive nitrosylation of the heme (*34*).

Mössbauer Spectroscopy. The Mössbauer spectra of HAO are complicated by the presence of a large number of heme irons in similar environments and by heme−heme interactions. A full understanding of the spectra is not within the scope of the present work, but the spectra are important indicators of changes in hemes. A spectrum of oxidized HAO at 150 K (Figure 5A) shows a broad quadrupole doublet which can be simulated with at least two low-spin species ($\delta_1 = 0.24$ mm/s, $\delta_2 = 0.18$ mm/s, $\Delta Eq_1 = 2.29$mm/s, $\Delta Eq_2 = 1.89$ mm/s). These parameters are typical of low-spin Fe(III) in heme. A previous Mössbauer study of HAO found only low-spin hemes for oxidized HAO (*35*). The addition of NO to HAO resulted in a slight sharpening of both lines. The weak absorption feature near zero velocity is difficult to assign, but it appears to originate from a high-spin Fe(III) impurity species, with parameters of $\delta = 0.48$mm/s and $\Delta Eq = 0.63$ mm/s. This species accounted for only 3% of the total iron (much less than one heme), and it was not affected by the addition of NO.

Figure 5B (solid line) shows low-temperature Mössbauer spectra of HAO in the presence of a small magnetic field. The broad features throughout the region from −4 to +5 mm/s are due to the paramagnetic features of low-spin ferric hemes. The doublet feature indicated by the bracket is at the quadrupole doublet of the iron and is due to the absence of a hyperfine field at the iron nucleus. This condition may arise either due to small principal axis *A*-values or from states in the exchange-coupled heme pairs which have a small magnetic moment. The addition of NO (Figure 5B, dot symbols) shows a decrease of in the wings of the spectrum near −4 and +5 mm/s, indicating a loss of paramagnetic iron. This is compensated by an increase in the absorption of a diamagnetic quadrupole doublet feature. The difference spectrum of NO minus oxidized HAO (Figure 5C) shows the new quadrupole doublet. A fit to this doublet is shown, with iron parameters of $\delta = 0.06$ mm/s and $\Delta Eq = 2.1$ mm/s. The relative area of the new doublet is 8%, which is less than that expected for one heme site (12.5%). However, the appearance of a new quadrupole doublet must be accompanied by the loss of signal in the oxidized sample. If the lost signal in the oxidized sample has a doublet feature

Table 1: Mössbauer Isomer Shift, Quadrupole Splitting, and Line Width (all in mm/s) for the NO Complex of Ferric Myoglobin

T (K)	δ	ΔEq	Γ
4.2	0.055	1.628	0.348
192	0.023	1.649	0.444

which overlaps with the new doublet, the perceived area of the new doublet would be diminished.

In our efforts to determine whether the Mössbauer parameters of the new species are indicative of Fe(III)NO, we found very few characterized ferric heme complexes of NO. In particular, no Mössbauer parameters have been published for the NO complex of ferric myoglobin or hemoglobin. Thus, we prepared a sample of the NO complex of ferric myoglobin. The Mössbauer spectrum of the sample showed one clean quadrupole doublet, indicative of a diamagnetic species, with the parameters given in Table 1. The sample will undergo reduction in the presence of excess NO after approximately 15 min due to reductive nitrosylation (*34*); thus the sample was frozen within 2 min of NO addition. The sample showed no evidence of reduced iron in the Mössbauer spectrum. Furthermore, an aliquot of the same sample was measured with EPR spectroscopy and found to contain no detectable Fe(II)−NO and less than 5% unligated Fe(III).

The characterized ferric NO complex octaethylporphyrin Fe(NO)(N-MeIm)Cl is diamagnetic and has Mössbauer parameters of $\delta = 0.02$ mm/s and ΔEq = 1.64 mm/s (*36*). The Mössbauer parameters of the ferric myoglobin NO and ferric heme NO complexes compare well with the new species in HAO, indicating that the new species is a diamagnetic ferric NO heme complex.

EPR Spectroscopy. EPR spectra of fully oxidized HAO are shown in Figure 6A for orientations of the microwave magnetic field $\mathbf{B}_1$ perpendicular and parallel to the static field **B**. All of the signals in these two spectra have been assigned in previous work (*11*). The resonances at $g = 1.35$, 2.2, and 3.1 are from four low-spin ferric hemes. The resonances at $g = 1.66$, 1.94, 2.8, and 3.4 and $g = 3.7$ (|| mode) are from an exchange-coupled heme pair, specifically hemes 3 and 5 of the crystal structure. The resonance at $g = 8$ (|| mode) is from a second pair of exchange-coupled hemes, specifically hemes P460 and 6, where heme P460 (heme 4) is the substrate binding site of the enzyme. All eight hemes per monomer of fully oxidized HAO are quantitatively assigned to these observed EPR signals.

The result of addition of NO to an anaerobic EPR sample of oxidized HAO is shown in Figure 6B. The spectrum for $\mathbf{B}_1 \perp \mathbf{B}$ is displayed as the difference of NO minus oxidized HAO. The subtraction factor was determined by minimization of the features at $g = 3.1$, 2.8, 1.66, and 1.35 of oxidized HAO. The large signal near $g = 1.9$ is typically observed in protein solutions from nonspecific binding of NO to the protein. The same signal is observed from an anaerobic NO-saturated solution of bovine serum albumin. The signal at $g = 2.2$ is present in various samples at varying intensities. If we assume that this $g = 2.2$ resonance is part of an EPR spectrum having *g*-tensor values of $g = 1.95$, 1.95, and 2.2 (chosen so as to be partially obscured by the nonspecific NO resonance), then signal quantitation indicates that the $g = 2.2$ species could account for no more than 20% of the monomeric protein concentration. The signal at $g = 3.4$ is weak but is consistently observed in all samples. For $\mathbf{B}_1 \parallel \mathbf{B}$ (Figure 6B), the EPR spectrum shows loss of the $g = 8$ signal. Since the $g = 8$ signal is associated with the hemes at the active site, the loss of this signal indicates that NO binds to HAO at heme P460.

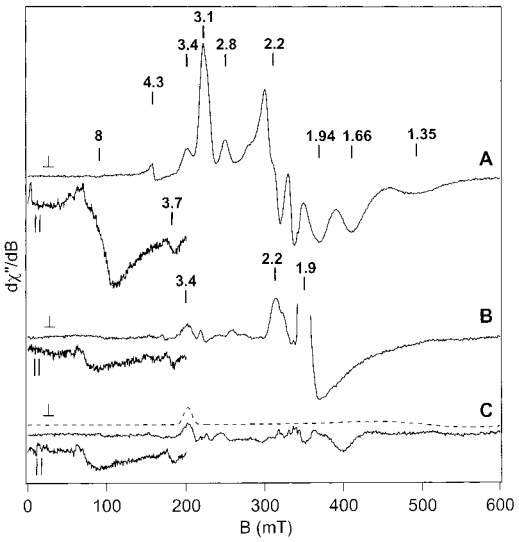

FIGURE 6: (A) EPR spectra of oxidized HAO for $\mathbf{B}_1 \perp \mathbf{B}$ and $\mathbf{B}_1 \parallel \mathbf{B}$. (B) Difference spectrum ($\perp$) of the NO adduct of HAO minus oxidized. (C) Difference spectrum ($\perp$) after purging a sample of NO. The || mode spectra for (B) and (C) are for the same respective samples, but are *not* difference spectra, and show loss of the $g = 8$ signal. The simulation in (C) (dashed line) is calculated for [$S = {}^1/_2$] = 0.45 mM with a *g*-tensor of 0.70, 1.35, and 3.4. Experimental conditions: [HAO] = 0.45 mM; microwave parameters, 9.62 GHz ($\perp$), 9.26 GHz (||), 0.2 mW; $T = 14$ K ($\perp$), 2 K (||). All spectra are displayed on the same vertical scale, except the parallel mode spectra are all at 5-fold higher gain. The signal at $g = 4.3$ is from an impurity Fe(III) species of less than 5% monomer concentration.

We have shown from the above FTIR and Mössbauer data that the binding of NO to HAO results in the formation of a diamagnetic $\{FeNO\}^6$ species. Thus, the P460 heme is no longer spin coupled to heme 6, and we should expect to find a new EPR signal from heme 6 which has spin $S = {}^1/_2$. In other words, the addition of one molecule of NO to an integer-spin system must give an overall half-integer spin system and a corresponding new EPR signal for $\mathbf{B}_1 \perp \mathbf{B}$. Conceivably, the adventitious NO signal at $g = 1.95$ could mask the appearance of new signals, such as a signal associated with the $g = 2.2$ resonance. For example, recent studies of a low-spin bis-isocyanide porphyrin complex give a novel low-spin EPR spectrum with $g = 1.94$, 2.2, and 2.2 (*37*). To determine if signals were masked, the NO was exchanged out of solution with multiple cycles of sample evacuation and Ar equilibration. Figure 6C show the resulting difference spectra of Ar minus oxidized for $\mathbf{B}_1 \perp \mathbf{B}$. The exchange with Ar resulted in the loss of the $g = 1.9$ and 2.2 signals but without recovery of the $g = 8$ resonance ($\mathbf{B}_1 \parallel \mathbf{B}$). Thus, the signal at $g = 2.2$ cannot be attributed to the heme partner but is from a paramagnetic minority species of unknown origin. The absence of the $g = 8$ signal after Ar exchange suggests that NO remains bound. Control experiments with oxidized HAO under an Ar atmosphere (without NO addition) resulted in no signal changes from the oxidized EPR spectrum. Exposure of the NO-bound sample to oxygen had no effect.

The addition of excess NO may result in the presence of other products that could also bind to ferric hemes. To test for this, the NO donor DEANO was added in 2-fold excess to HAO and frozen after 7 min. The delivered NO amount calculated using the 16 min half-life for the donor agent gave a ratio of NO to HAO of 0.5:1. The resulting parallel mode spectrum showed loss of the $g = 8$ signal and a perpendicular mode difference spectrum similar to that of Figure 6C. We suspect the amount of NO delivered was higher than 0.5 equiv per HAO. The amount of NO delivered was less than 1 equiv per HAO as indicated by the absence of an EPR signal from nonspecific NO binding.

We are forced to consider that the weak signal at $g = 3.4$ originates from heme 6 after NO addition. EPR signals from single heme sites with $g_{max} > 3.2$ are not commonly observed and are referred as large g_{max} hemes or highly anisotropic low-spin (HALS) hemes (*38*, *39*). Moreover, the signal intensity also is consistent with the assignment. A normal heme signal would contribute far too much signal intensity to account for the weak signal intensity. We make the assumption that the full *g*-tensor of this signal is 0.70, 1.35, and 3.4, which are possible *g*-values of a large g_{max} heme complex (*40*). A quantitative simulation for these *g*-values is overlaid in Figure 6C, where the intensity scale of the simulation is determined from the protein concentration. The simulation matches the data reasonably well. Thus, heme 6 does produce a signal of the correct intensity when uncoupled from P460, although intrinsically very weak due to the broad magnetic field span of the signal. The addition of cyanide to HAO results in the loss of the $g = 8$ signal, indicating binding of cyanide (*15*); however, the $g = 3.4$ signal is not observed. This is consistent with a paramagnetic P460−CN complex which is spin coupled to heme 6 and thus does not produce a readily observable EPR signal.

The samples in the presence of NO and after Ar exchange both show the same $g = 3.4$ signal and absence of the $g = 8$ signal, suggesting that NO remains bound even after rigorous removal of NO from solution. The nonspecific NO signal at $g = 1.9$ vanished after the first exchange with Ar. Two additional similar exchanges with Ar on the same sample did not change the EPR signals further. Previous reports have shown that Fe(III) heme−NO complexes will undergo photodissociation (*41*). The sample of Figure 6C was subjected to intense illumination with white light (300 W projection bulb) while in a room temperature water bath and additional exchanges with Ar during illumination. After this treatment, the $g = 8$ signal ($\mathbf{B}_1 \parallel \mathbf{B}$) and the fully oxidized HAO spectrum ($\mathbf{B}_1 \perp \mathbf{B}$) were recovered. Thus, consistent with the FTIR spectroscopic results stated above, NO can be removed to recover the initial oxidized HAO state.

Effect of Substrate and NO on HAO. In previous work, the addition of the substrate hydroxylamine results in the loss of EPR signals from the heme at $E_m = +288$ mV ($g = 3.1$) and partial reduction of hemes 3 and 5 both at $E_m \sim 0$ mV ($g = 3.4$, 2.8, 1.94, 1.66). In addition, the $g = 8$ EPR signal from the active site (hemes P460 and 6) vanishes (*15*). In the presence of hydroxylamine, we have observed a new signal (shown in Figure 7B) which is approximately axial with *g*-values of 2.01 and 2.11 and displays a ^{14}N hyperfine triplet pattern with a coupling constant of 1.7 mT. This signal is very similar to those observed from 5-coordinate ferrous heme−NO complexes {FeNO}^{7} for which the bond to the axial His is lost (*31*). Spin quantitation indicates that this signal in HAO is a minority species of less than 5% of the monomer protein concentration. The addition of saturating amounts of NO and hydroxylamine to HAO results in a significant increase in this signal. However, spin quantitation found that the amounts are always substoichiometric, never exceeding 50% of monomeric subunit concentration. The addition of hydrazine to HAO did not generate the 5-coordinate heme−NO signal, indicating that this signal is unique to the hydroxylamine.

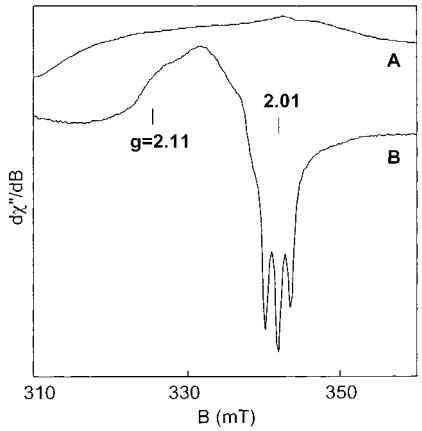

FIGURE 7: EPR spectra of HAO in the (A) absence and (B) presence of substrate NH_2OH. Experimental conditions: [HAO] = 1.5 mM; microwave parameters, 9.64 GHz, 0.2 mW; $T = 14$ K; modulation, 0.15 mT.

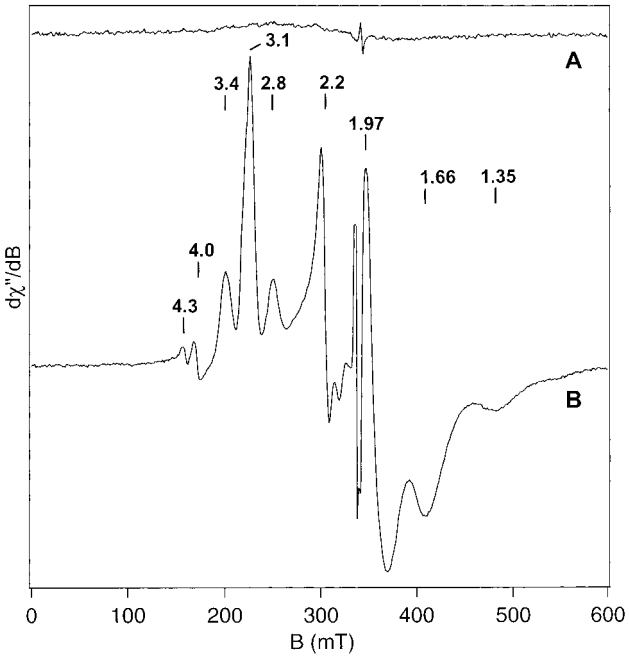

FIGURE 8: EPR spectra of (A) dithionite-reduced HAO and (B) dithionite-reduced HAO plus NO. Experimental conditions: [HAO] = 0.48 mM; [$Na_2S_2O_4$] = 5 mM; microwave parameters, 9.62 GHz, 0.2 mW; $T = 14$ K.

The difficulty in stabilizing a stoichiometric amount of the heme−NO complex is due to oxidation of HAO by NO. A sample of HAO degassed with Ar and reduced with $Na_2S_2O_4$ showed loss of the EPR signals for both $\mathbf{B}_1 \perp \mathbf{B}$ (Figure 8A) and $\mathbf{B}_1 \parallel \mathbf{B}$ (not shown). The spectrum of Figure 8B is the sample in Figure 8A after anaerobic addition of NO. The NO addition resulted in recovery of most of the oxidized HAO heme signals. The EPR signal from the E_m

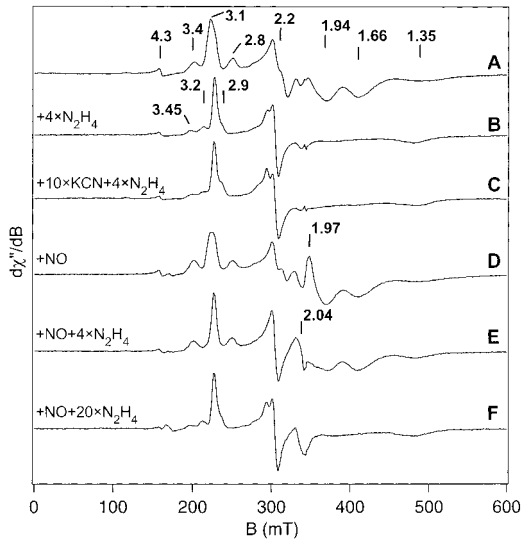

FIGURE 9: EPR spectrum of (A) oxidized HAO and in the presence of (B) 2 mM hydrazine, (C) 5 mM KCN + 2 mM hydrazine, (D) saturated NO solution, (E) NO + 2 mM hydrazine, and (F) NO + 10 mM hydrazine. Experimental conditions: [HAO] = 0.48 mM; microwave parameters, 9.62 GHz, 0.2 mW; $T = 14$ K.

= +288 mV heme is partially recovered, and the $g = 8$ signal is not observed, indicating that NO is bound to heme P460.

Figure 9 shows the results of the addition of the substrate hydrazine and inhibitors to HAO. The addition of a 4-fold excess of hydrazine to oxidized HAO (Figure 9B) results in the loss of the same EPR signals as with hydroxylamine; however, the signals from hemes 3 and 5 ($E_m \sim 0$ mV, $g =$ 3.4, 2.8) are now completely absent. This is apparently a result of the lower reduction potential of hydrazine relative to hydroxylamine. The reduction potentials at pH 7 for the oxidation of NH_2OH to N_2O and N_2H_4 to N_2 are −0.46 and −0.64 V, respectively, for values calculated from the standard reduction potentials at pH 0 (*42*). Three signals of unknown origin and weak in intensity appear at $g = 3.45$, 3.2, and 2.9 in the presence of hydrazine. The 3.2 and 2.9 signals have been observed previously (*43*, *44*). The $g =$ 3.45 signal could possibly be the large g_{max} EPR signal from heme 6. However, it is not yet possible to isolate this signal and compare accurately to the signal observed in the presence of NO (Figure 6B). Thus, we currently cannot assign this signal to heme 6 with certainty.

The presence of a 10-fold excess of cyanide prior to addition of hydrazine results in the same state of the enzyme as without cyanide, as shown in Figure 9C. The experiment was repeated with a saturated anaerobic NO solution in place of cyanide. The EPR spectrum of oxidized HAO + NO (Figure 9D) shows the typical HAO signals and a signal from nonspecific NO at $g = 1.97$. Upon addition of a 4-fold excess of hydrazine (Figure 9E), the 0 mV hemes become partially reduced and the nonspecific NO signal at $g = 1.97$ is nearly absent. A new weak signal is present at $g = 2.04$, which quantifies to less than 5% of the protein concentration. The origin of this signal is uncertain, possibly a low-spin Fe(III) species. This signal does not display the triplet hyperfine pattern of Figure 7B. Additional hydrazine (Figure 9F) results in full reduction of the 0 mV hemes, giving nearly the same spectrum as in Figure 9B. Control experiments with only NO and hydrazine show no loss of the $g = 1.97$ signal and thus no direct reaction of NO and hydrazine on the time scale of a few minutes. Thus, NO has been consumed by HAO in the presence of hydrazine. Upon consumption of all NO, the additional hydrazine reduces the enzyme to the same state as without NO.

Similar results are observed from the optical spectra shown in Figure 3B. When NO is present prior to the addition of hydrazine, only the heme at $E_m = +288$ mV becomes reduced (Figure 3B, solid line). The hemes at 0 mV are not reduced due to consumption of the hydrazine by NO. When the order of mixing is changed and NO is added to the cuvette containing HAO and hydrazine, initially HAO becomes substantially reoxidized. After several minutes, gradual rereduction of HAO occurs (Figure 3B, dashed line) but not to the same level of reduction seen in the absence of NO (Figure 3B, dotted line).

Cytochrome c_{554} is the physiological electron acceptor for HAO. When an aliquot of NO-saturated buffer is added or NO gas is bubbled through a solution of cytochrome c_{554} and HAO, no reduction of either protein is observed, again indicating that NO is not oxidized by HAO.

DISCUSSION

The FTIR and Mössbauer spectroscopies unambiguously indicate that NO binds to a heme Fe. The IR band energy 1920 cm^{-1} is typical of $\{FeNO\}^6$ heme proteins complexes possessing a linear FeNO unit. This energy is near that observed for the nitrosyl complex of ferric myoglobin (1922 cm^{-1}) (*29*). The Mössbauer data indicate that only one Fe is affected and that binding of NO causes loss of a paramagnetic iron species and the appearance of a $\{FeNO\}^6$ species which is diamagnetic ($S = 0$). Heme P460 does not display a typical ferric heme EPR signal. Instead, due to an exchange coupling with heme 6, an EPR signal is observed at $g = 8$ for $\mathbf{B_1} \parallel \mathbf{B}$ (*15*). We find that the $g = 8$ signal vanishes upon NO addition, which indicates that NO binds to heme P460. Heme P460 is the only 5-coordinate metal center, and the binding of NO must change the spin state and therefore the EPR signal vanishes.

The coordination of NO to heme P460 results in the formation of a diamagnetic iron complex. This results in the loss of the spin interaction between heme P460 and heme 6, and a new EPR signal must therefore be observed from the spin $S = {}^1/_2$. The NO complex thus allows, for the first time, the detection of a signal from heme 6. The signal from heme 6 can only be interpreted as a large g_{max}-type heme species. As is evident in the structure shown in Figure 2, the planes of the imidazole rings which are coordinated to heme 6 are orthogonal (His204, His263). No other heme in HAO displays this orthogonal imidazole geometry. Consistent with this assignment, an orthogonal imidazole geometry has been shown in a number of other characterized heme complexes to give rise to large g_{max}-type EPR signals (*39*, *45*). These conclusions strengthen our original findings in which P460 and heme 6 are exchange coupled.

The oxidized state of HAO prior to addition of NO could be recovered after Ar exchange and illumination, but it is unclear why illumination is necessary. We have shown that NO was removed from solution by the loss of the $g = 1.97$ EPR signal from NO. We can detect a minimum concentration of NO at approximately 10^{-5} M, but our gas exchange procedure should have given [NO] < 10^{-5} M. The dissocia-

tion rates for NO to typical ferric hemes are sufficiently fast ($k_{off} = 10^1-10^2$ s^{-1}) and the binding constant is sufficiently small ($K_{eq} = 10^3-10^5$ M^{-1}) (*41*, *46*) that a significant fraction of uncomplexed HAO should have been observed. Thus, we should observe recovery of the original oxidized state without illumination. We conclude that the equilibrium constant for the association of NO to heme P460 (a unique heme environment) is 10^5 M^{-1} or higher. Alternatively, NO^+ leaves, heme P460 is reduced, and the illumination results in photooxidation of heme P460. However, in this process, we might expect a change to the $g = 3.4$ signal, or a new radical signal, or reduction of an iron after photooxidation of heme P460, but none of this is observed.

Catalytic Cycle. Oxidation of substrate presumably occurs after binding of NH_2OH to heme P460, rather than oxidation at an outer sphere site. The combined EPR and optical data of HAO in the presence of NH_2OH indicate the stabilization of either a substrate-bound complex or a bound intermediate oxidation product. In the oxidized or reduced states of uncomplexed HAO, heme P460 shows characteristic EPR or optical features. Since, as shown here, these features are not observed in the presence of NH_2OH, some as yet unknown type of substrate or intermediate complex must be present. The addition of NH_2OH to HAO produces a small amount (<5%) of a NO−ferrous heme intermediate complex. However, the low yield and requirement of high substrate concentration suggest that this species is not part of the catalytic cycle. The addition of NO only results in oxidation of HAO, and thus NO is reduced, most likely to N_2O. We conclude that NO is not a long-lived intermediate.

The accumulating evidence suggests that NO is not an intermediate in the catalysis of nitrite production by HAO and supports the model of formation of NO^+ by removal of a hydride or two electrons in concert. We note two unique elements of catalysis in HAO. First, catalysis takes place at a heme (where the substrate binds the Fe) and involves the net outflow of electrons from substrate and then from the heme and enzyme. All other heme enzyme redox chemistry is overall reductive as O_2 or H_2O_2 is reduced to H_2O (monooxygenase, oxidase, peroxidase) or nitrite or sulfite is reduced (*47*). Second, a meso ring carbon of the catalytic heme of HAO is covalently cross-linked to a ring carbon of an aromatic residue (tyrosine). Though we cannot say how, we suppose these properties, together with the large pool of accessory electron-accepting hemes, are related. The catalyst may be designed to ensure effective irreversible removal of electrons in two-electron steps.

In contrast to P460 of HAO, many heme proteins (e.g., hemoglobin) are reduced in the presence of excess NO via reductive nitrosylation (*34*, *48*). That this does not occur in HAO is likely due to the relatively low reduction potential of the P460 heme of HAO and is an important property of the active site of HAO. The low heme potentials of the active site (−260, −190 mV) favor donation of electrons to the other hemes of HAO, promoting charge separation away from N-containing intermediates and products and into the respiratory chain. A long-lived intermediate might react with substrate or other byproducts to yield less than four electron equivalents per substrate.

NO appears to bind tightly to heme P460, and only upon rigorous depletion of NO from solution can we stop formation of the FeNO complex. This is a potential problem for enzymatic function since NO can also be a product of HAO (*21*). However, we have shown that the enzyme can recover from the NO-bound state. Substrate is able to partially reduce HAO in the presence of either cyanide or NO, and NO will oxidize HAO. Moreover, substrate and HAO will consume NO from solution. These results indicate an alternative pathway for heme reduction of HAO by substrate in the presence of inhibitors. Given the high reduction potential of at least one heme (+288 mV), it is possible that substrate interaction occurs through an outer-sphere mechanism at a heme other than heme P460. Another possibility might involve substrate oxidation at an active site on one subunit, followed by electron transfer across subunits and reduction of NO at an inhibited active site.

REFERENCES

1. Hooper, A. B., Vannelli, T., Bergmann, D. J., and Arciero, D. M. (1997) *Antonie van Leeuwenhoek 71*, 56−67.
2. Hooper, A. B., and Nason, A. **(**1965) *J. Biol. Chem. 240*, 4044−4057.
3. Andersson, K. K., and Hooper, A. B. (1983) *FEBS Lett. 164*, 236−240.
4. Schalk, J., de Vries, S., Kuenen, J. G., and Jetten, M. S. M. (2000) *Biochemistry 39*, 5405−5412.
5. Terry, K., and Hooper, A. B. (1981) *Biochemistry 20*, 7026−7032.
6. Igarashi, N., Moriyama, H., Fujiwara, T., Fukumori, Y., and Tanaka, N. (1997) *Nat. Struct. Biol. 4*, 276−284.
7. Arciero, D. M., and Hooper, A. B. (1993) *J. Biol. Chem. 268*, 14645−14654.
8. Iverson, T. M., Arciero, D. M., Hsu, B. T., Logan, M. S. P., Hooper, A. B., and Rees, D. C. (1998) *Nat. Struct. Biol. 5*, 1005−1012.
9. Einsle, O., Messerschmidt, A., Stach, P., Bourenkov, G. P., Bartunik, H. D., Huber, R., and Kroneck, P. M. H. (1999) *Nature 400*, 476−480.
10. Arciero, D. M., Golombek, A., Hendrich, M. P., and Hooper, A. B. (1998) *Biochemistry 37*, 523−529.
11. Hendrich, M. P., Petasis, D., Arciero, D. M., and Hooper, A. B. (2001) *J. Am. Chem. Soc. 123*, 2997−3005.
12. Hooper, A. B. (1989) in *Autotrophic Bacteria* (Schlegel, H. G., and Bowien, B., Eds.) pp 239−265, Science Tech Publishers, Madison, WI.
13. Arciero, D. M., Balny, C., and Hooper, A. B. (1991) *Biochemistry 30*, 11466−11472.
14. Hooper, A. B., and Terry, K. R. (1977) *Biochemistry 16*, 455−459.
15. Hendrich, M. P., Logan, M., Andersson, K. K., Arciero, D. M., Lipscomb, J. D., and Hooper, A. B. (1994) *J. Am. Chem. Soc. 116*, 11961−11968.
16. (a) Logan, M. S. P., Balny, C., and Hooper, A. B. (1995) *Biochemistry 34*, 9028−9037. (b) Logan, M. S. P., and Hooper, A. B. (1995) *Biochemistry 34*, 9257−9264.
17. Arciero, D. M., Hooper, A. B., Cai, M., and Timkovich, R. (1993) *Biochemistry 32*, 9370−9378.
18. Andersson, K. K., Kent, T. A., Lipscomb, J. D., Hooper, A. B., and Münck, E. (1984) *J. Biol. Chem. 259*, 6833−6840.
19. Andersson, K. K., Babcock, G. T., and Hooper, A. B. (1991) *Biochem. Biophys. Res. Commun. 174*, 358−363.
20. Hooper, A. B., Terry, K. R., and Maxwell, P. C. (1977) *Biochim. Biophys. Acta 462*, 141−152.
21. Hooper, A. B., and Terry, K. R. (1979) *Biochim. Biophys. Acta 571*, 12−20.
22. Hooper, A. B., and Balny, C. (1982) *FEBS Lett. 144*, 299−303.
23. Hooper, A. B., Debey, P., Andersson, K. K., and Balny, C. (1983) *Eur. J. Biochem. 134*, 83−87.
24. Hooper, A. B. (1968) *Biochim. Biophys. Acta 162*, 49−65.

25. Ritchie, G. A. F., and Nicholas, D. J. D. (1974) *Biochem. J. 138*, 471−480.
26. Yamanaka, T., Shinra, M., Takahashi, K., and Shibasaka, M. (1979) *J. Biochem. (Tokyo) 86*, 1101−1108.
27. Richter-Addo, G. B., and Legzdins, P. (1992) in *Metal Nitrosyls*, Oxford University Press, New York.
28. Maxwell, J. C., and Caughey, W. S. (1976) *Biochemistry 15*, 388−396.
29. Miller, L. M., Pedraza, A. J., and Chance, M. R. (1997) *Biochemistry 36*, 12199−12207.
30. Salerno, J. C. (1996) in *Nitric Oxide: Principles and Actions* (Lancaster, J., Jr., Ed.) Chapter 2, Academic Press, New York.
31. Palmer, G. (1978) in *The Porphyrins* (Dolphin, D., Ed.) Vol. 4, Chapter 6, Academic Press, New York.
32. Debrunner, P. G. (1989) in *Iron Porphyrins* (Lever, A., and Gray, H., Eds.) Part 3, pp 137−234, VCH Publishers, New York.
33. Enemark, J. H., and Feltham, R. D. (1974) *Coord. Chem. Rev. 13*, 339−406.
34. Wang, Y., and Averill, B. A. (1996) *J. Am. Chem. Soc. 118*, 3972−3973.
35. Lipscomb, J. D., Andersson, K. K., Münck, E., Kent, T. A., and Hooper, A. B. (1982) *Biochemistry 21*, 3973−3976.
36. Schünemann, V., Benda, R., Trautwein, A. X., and Walker, F. A. (2000) *Isr. J. Chem. 40*, 9−14.
37. Walker, F. A., Nasri H., Turowska-Tyrk, I., Mohanrao, K., Watson, C. T., Shokhirev, N. V., Debrunner, P. G., and Scheidt, W. R. (1996) *J. Am. Chem. Soc. 118*, 12109−12118.
38. Palmer, G. (2000) in *Physical Methods in Bioinorganic Chemistry* (Que, L., Jr., Ed.) pp 121−185, University Science Books, Sausalito, CA.
39. Walker, F. A., Boi Hanh H., Scheidt, W. R., and Osvath, S. R. (1986) *J. Am. Chem. Soc. 108*, 5288−5297.
40. (a) Palmer, G. (1985) *Biochem. Soc. Trans. 13*, 548−560. (b) Salerno, J. C. (1985) *Biochem. Soc. Trans. 13*, 611−615.
41. Hoshino, M., Ozawa, K., Seki, H., and Ford, P. C. (1993) *J. Am. Chem. Soc. 115*, 9568−9575.
42. Bard, A. J., Parsons, R., and Jordan, J., Eds. (1985) in *Standard Potentials in Aqueous Solution*, p 138, Marcel Dekker, New York.
43. Lipscomb, J. D., and Hooper, A. B. (1982) *Biochemistry 21*, 3965−3972.
44. Prince, R., and Hooper, A. B. (1987) *Biochemistry 26*, 970−974.
45. Munro, O. Q., Serth-Guzzo, J. A., Turowska-Tyrk, I., Mohanrao, K., Shokhireva, T. Kh., Walker, F. A., Debrunner, P. G., and Scheidt, W. R. (1999) *J. Am. Chem. Soc. 121*, 11144−11155.
46. (a) Sharma, V. S., Traylor, T. G., Gardiner, R., and Mizukami, H. (1987) *Biochemistry 26*, 3837−3843. (b) Traylor, T. G., and Sharma, V. S. (1992) *Biochemistry 31*, 2847−2849.
47. Arciero, D. M., and Hooper, A. B. (1998) *Biochem. Soc. Trans. 26*, 385−389.
48. Averill, B. A. (1996) *Chem. Rev. 96*, 2951−2964.

BI011332Z